Available online at www.sciencedirect.com
ScienceDirect
Journal of the European Ceramic Society 27 (2007) 4515–4520
www.elsevier.com/locate/jeurceramsoc

The mechanism of the low-temperature formation of barium hexaferrite

Darja Lisjak *, Miha Drofenik

Jožef Stefan Institute, Advanced Materials Department, 1000 Ljubljana, Slovenia

Received 8 November 2006; received in revised form 7 February 2007; accepted 18 February 2007
Available online 2 April 2007

Abstract

We have investigated the formation of barium hexaferrite via the coprecipitation method. Fine precursor powders were obtained with coprecipitation from water and ethanol solutions of various reagent salts. The coprecipitates were calcined at 300–800 °C for 0–50 h. The samples were characterized with X-ray powder diffraction, thermal analysis, electron microscopy and magnetometry. The formation of barium hexaferrite was a combination of two competing mechanisms and was not influenced by the reagent salts or the solvent. The formation temperature of the barium hexaferrite was reduced to 500 °C by optimizing the coprecipitation conditions.

Keywords: Powders-chemical preparation; Powders-solid state reaction; Magnetic properties; Ferrites; Hexaferrites

1. Introduction

As a result of its specific magnetic properties barium hexaferrite and its derivatives can be used for permanent magnets, magnetic recording media and microwave applications. The best-known representative of the hexaferrite family, barium hexaferrite, has the chemical formula $BaFe_{12}O_{19}$ (BaM). BaM has a magnetoplumbite structure with a close-packed oxygen lattice.[1] Ba ions replace O ions on specific positions, resulting in a particular sequence of O- and Ba–O-mixed layers. The smaller metal cations occupy the interstitial positions. The most significant property of BaM, its magnetocrystalline anisotropy, originates from the highly anisotropic crystal structure. In addition, the grain growth of such structures is also anisotropic, with a typical hexagonal plate-like morphology, which gives rise to a shape anisotropy. As a consequence, BaM exhibits the high coercivity required for permanent magnets.[2] Fine hexaferrite powders with a moderate coercivity are suitable for magnetic-recording media.[3] Moreover, due to their high anisotropy field, hexaferrites can be used at much higher frequencies than spinel ferrites or garnets. For this reason they are interesting for applications above 30 GHz.[4] Low-loss materials for microwave applications need to be defect free, from the compositional, the structural and the microstructural points of view. Finer starting powders exhibit a superior sintering behaviour than coarser powders, resulting in lower sintering temperatures and denser ceramics.[5] In addition, the number of structural defects can be decreased by the use of finer powders, which can be prepared at lower temperatures than coarser powders.[6]

Various methods have been reported for the preparation of fine hexaferrite powders: chemical coprecipitation,[7–9] sol–gel[10,11] and others.[12–19] Although none of these methods enable the formation of BaM at room temperature, its formation temperature is lower than for the classic solid-state reaction, in which BaM is formed indirectly via $BaFe_2O_4$. The formation of BaM normally involves the degradation of $BaCO_3$. $BaCO_3$ is either present in the initial reaction mixture[13,20] or it is formed from precursors during the preparation process.[9] The formation of $BaFe_2O_4$ and BaM starts with the degradation of $BaCO_3$ at 700–900 °C.[9,13,20] The preparation methods by which the formation of $BaCO_3$ was more or less successfully prevented are based on relatively complex procedures.[6,11,19] We showed previously that the formation of BaM is possible at temperatures as low as 500 °C.[21,22]

Here we report on the formation mechanism of BaM via coprecipitation. In order to elucidate the origin of the low-temperature formation of BaM from ethanol solutions we have conducted a thorough research on the influence of reagent salts and solvents. The coprecipitation conditions proved to have no influence on the formation mechanism of BaM, and it will be

* Corresponding author. Tel.: +386 1 4773 872; fax: +386 1 4773 875.
E-mail address: darja.lisjak@ijs.si (D. Lisjak).

0955-2219/$ – see front matter © 2007 Elsevier Ltd. All rights reserved.
doi:10.1016/j.jeurceramsoc.2007.02.202

shown that suppression of the formation of $BaCO_3$ resulted in the low-temperature formation of BaM.

2. Experimental procedure

The samples were prepared via coprecipitation, as described in detail previously.[22] Stoichiometric amounts of Ba and Fe salts – $BaCl_2$ (Ventron, ultrapure, Lot No. 044770307) or $Ba(NO_3)_2$ (Alfa Aesar, 99.995% metals basis, Lot No. 22331) and $FeCl_3$ (Alfa Aesar, 98%, anhydrous, Lot no. K05J02) or $Fe(NO_3)_3$ (Alfa, AR, Lot No. BA08255) – were dissolved in water or in a 75 vol.% solution of ethanol in water. The ethanol solution will be referred to as ethanol in the rest of this manuscript. The Ba^{2+} and Fe^{3+} concentrations in the starting solutions (with pH ≤ 1) were 0.06 and 0.74 mol/l, respectively. The obtained solutions of Ba–Fe salts were added to a NaOH solution (in water or in ethanol) with pH 13. After that the overall pH decreased and was corrected to a minimum value of 13 with a NaOH solution. The coprecipitation conditions we used are listed in Table 1. Dried, coprecipitated precursors were calcined at 300–800 °C for 0–50 h with heating and cooling rates of 10 K/min. The calcination time 0 h refers to the case when a sample was quenched by pulling from the furnace onto a cold metal plate immediately after reaching the final temperature.

The synthesis was monitored with thermogravimetric and differential thermal analysis (TGA and DTA) with heating and cooling rates of 2–20 K/min using a TG/DT analyzer (Netzsch STA 429 system) with a Pt crucible, and X-ray powder diffraction (XRD) using a diffractometer with Cu Kα radiation (D4 Endeavor, Bruker AXS, Karlsruhe, Germany). Additional experiments used simultaneous TG-DTA/DSC apparatus with the Gas Analytical System QMS 403 C Aëolos (STA 449 C/6/G Jupiter®-QMS 403 C). The microstructures of the powders were observed using a transmission electron microscope (TEM, Jeol-2000FX). The magnetic properties of the calcined powders were measured using a magnetometer (Drusch & Cie Voltreg 1.4 T) and the magnetization values (M) reported here were measured in a maximum magnetic field of 1.2 T.

The kinetic parameters, reaction rate constant (k) and reaction order (n), were determined by fitting various kinetic models to $\alpha = \alpha(t)$ curves, where α is a fraction of the product (BaM). Since the magnetization is directly proportional to the mass of the BaM the ratio M/M_{max} was taken as a quantitative measure of α. M is the magnetization of a sample, calcined at a particular temperature for a particular time, measured at 1.2 T, and M_{max} is the maximum M measured for the sample. The detection limit for the BaM using our magnetometer was 0.2 wt.%, which is approximately 10× lower than the detection limit of the XRD.

Table 1
Coprecipitation conditions

Sample	Reagent salts	Solvent
Wcl[a]	Chlorides	Water
ETcl	Chlorides	Ethanol
ETni	Nitrates	Ethanol

[a]Final washing step with absolute ethanol.

The activation energy (E_a) for the formation of BaM was determined in two ways: (1) from k values determined at different temperatures using the Arrhenius equations (1)[23] and (2) from DTA curves measured at different heating rates using Eq. (2).[24] Here, R is the general gas constant (8.314 g/mol K), h stands for the heating rate, T_m for the temperature corresponding to the maximum of the DTA peak, while A and C' are constants:

$$\ln k = \ln A - \frac{E_a}{RT} \quad (1)$$

$$\log h = -\frac{E_a}{4.57}\frac{1}{T_m} + C' \quad (2)$$

3. Results

3.1. The influence of the preparation conditions on the magnetization

The formation of $BaFe_{12}O_{19}$ (BaM) during the thermal treatment of the precursors obtained via the coprecipitation of Fe^{+3} and Ba^{2+} salts in alkaline media was monitored with XRD analysis (The exact details are reported in Ref. 22) and with magnetic measurements. The magnetization of the samples calcined below 500 °C was negligible and there was no evidence of BaM peaks in the XRD patterns of these samples. The crystallization of BaM started at 500 °C (Fig. 1, Table 2). There was no evidence of other magnetic phases that could contribute to the measured magnetization. Fig. 1 shows the room-temperature magnetization (M) measured at 1.2 T of the ETcl samples calcined at 500–800 °C. The M values increased with the calcination time up to ∼54 emu/g, and then stabilized at this value. This indicates that the crystallization of BaM was completed at that point. However, the M values of the samples calcined at 500 °C were lower than 50 emu/g. BaM did not crystallize completely in the samples calcined at 500 °C, not even after 50 h of calcination; however, it crystallized completely after 5 h when calcined at 600 °C and after only 1h when calcined at 700 or 800 °C. It is evident that the calcination temperature strongly influenced the formation rate of BaM.

A similar increase in the magnetization (M) was measured for the other samples, Wcl and ETni (Table 2). In general, the M values of the ETni samples were lower than those of the other samples. This is in accordance with the XRD data: $BaCO_3$ or $BaFe_2O_4$ were detected in all the ETni samples. $BaCO_3$

Table 2
Measured magnetizations of the Wcl and ETni samples at 1.2 T (M)

Sample	Calcination temperature (°C)	M (emu/g), 1 h calcinations	M (emu/g), 10 h calcination
Wcl	500	2.3	31
	600	47	53
	700	52	57
	800	56	55
ETni	500	6	36
	600	33	49
	700	45	
	800	45	46

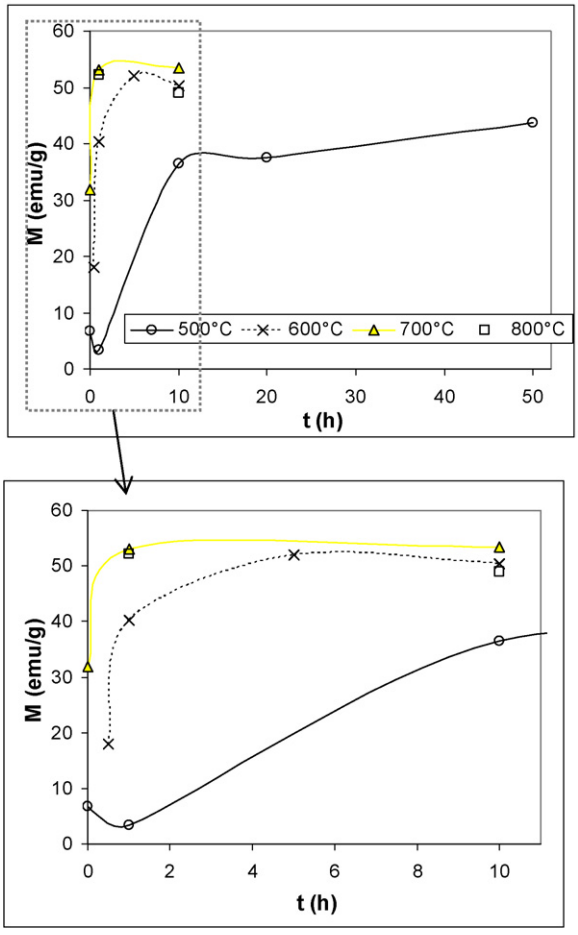

Fig. 1. Magnetization (M), measured at 1.2 T, of the ETcl samples with the respect to calcination time (t) and temperature.

as a diamagnetic impurity and $BaFe_2O_4$ as a paramagnetic impurity dilute the ferrimagnetic BaM and consequently lower the magnetization. In contrast to the ETni samples, only BaM was detected in the ETcl samples when calcined at $\geq$600 °C. Although a minor hematite peak was observed in the XRD patterns of all the Wcl samples they exhibited a similar M to the ETcl samples.

3.2. Thermal analysis

The TGA/DTA curves of the as-coprecipitated ETcl measured at a heating rate of 10 K/min are shown in Fig. 2. Based on the XRD analysis the processes associated with the observed DTA peaks can be explained as follows. A huge endothermic peak with a minimum around 131 °C is associated with a huge mass loss due to the evaporation of water. A minor exothermic peak, also associated with a significant mass loss, can be observed at around 288 °C. This peak can be attributed to the formation of α-Fe_2O_3. Although at this temperature γ-Fe_2O_3 could form[19] we found no such evidence from the XRD analysis or from the magnetic measurements. The mass loss up to 600 °C is around 20%. This observed mass loss can be attributed to the degradation of the hydroxide precursors and the consequent evaporation of H_2O. At 600–700 °C an additional mass

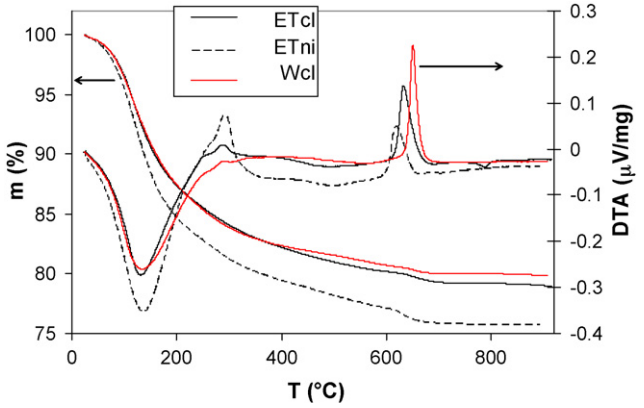

Fig. 2. TGA/DTA curves of the as-coprecipitated samples, measured at a heating rate of 10 K/min: full black line (ETcl), broken black line (ETni), and gray full line (Wcl).

loss of 1% was detected in the ETcl sample. This was attributed to the reaction of intermediates and the final degradation of the precursors involved in the associated chemical reactions, i.e., the temperature of the mass stabilization coincides with the temperature of the termination of the chemical reactions in the samples. A pronounced exothermic peak with a maximum at 633 °C is associated with the 0.9% mass loss and corresponds to the formation of BaM.

Similar TGA/DTA behaviour was observed for the other two samples (also shown in Fig. 2) with a slight difference in the temperatures of the DTA peaks and in the mass loss. The Wcl precursors did not exhibit a clear exothermic peak associated with the formation of α-Fe_2O_3. This peak was much more pronounced for the ETni precursor.

There is a notable difference between the formation temperature of the BaM determined from the magnetization and the XRD (500 °C) and the formation temperature of the BaM determined from the DTA (>600 °C). This can be partly explained by the long calcination times that were applied in the first case, and it was confirmed with the DTA measurements performed at various heating rates, 2–20 K/min. As shown in Fig. 3 the temperature of the corresponding maximum of the BaM DTA peaks decreased with the decreasing heating rate. When the

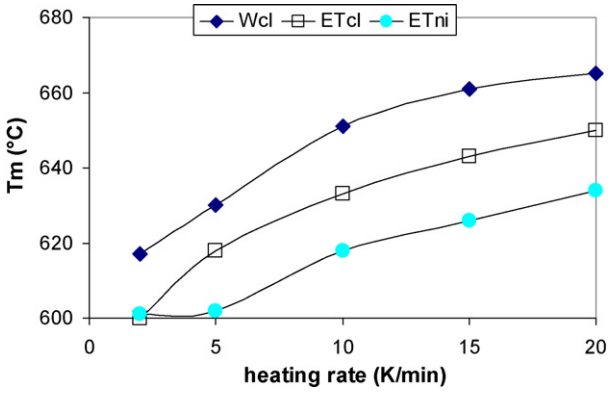

Fig. 3. Dependence of the maximum temperature (T_m) of the DTA peak related to the formation of BaM on the heating rate.

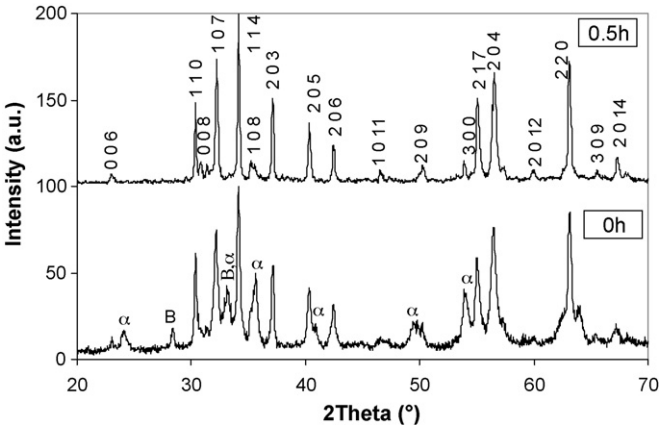

Fig. 4. XRD diffractograms of the ETcl samples calcined at 700 °C. α and B correspond to the α-Fe_2O_3 and $BaFe_2O_4$ structures, respectively. Other peaks correspond to the $BaFe_{12}O_{19}$ structures and are indexed according to the $P6_3/mmc$ (194) space group.

heating rate was decreased to 2 K/min, the temperature of the DTA peak decreased to 600 °C. The 600 °C was also determined as the minimum temperature required for the complete crystallization of BaM (see Section 3.1). Additional evidence and an explanation are given in Section 4.2. Nevertheless, we can conclude that the formation of BaM is strongly kinetically dependent.

4. Discussion

4.1. The mechanism of BaM formation

The formation of BaM started at lower temperatures and the final reaction was accomplished at a higher temperature. Such a sluggish process of BaM formation results from the appearance of $BaCO_3$ and consequently of $BaFe_2O_4$ in the early stage of the reaction, since their formation was not completely prevented. $BaCO_3$ was detected in the aged coprecipitates and in the samples calcined below 500 °C (or even at 600 °C for the ETni samples). The XRD analysis of the quenched samples (0 h) revealed the formation of $BaFe_2O_4$, even in the ETcl (Fig. 4) and the Wcl samples. No such evidence was reported previously.[7,8,21,22] The reason for this discrepancy is the calcination time. The older data included only samples calcined for a minimum of 1 h. Fig. 4 shows that a calcination time of only 0.5 h resulted in $BaFe_2O_4$-free powder. Finally, the similar TGA/DTA behaviours of all the precursors indicate the same mechanism of BaM formation using the described coprecipitation procedure. Based on all the presented data we can summarize the main chemical reactions associated with the formation of the BaM in Eqs. (3)–(8)):

$$BaA_2 + 12FeA_3 \xrightarrow{NaOH,\ H_2O,\ alcohol} Ba\text{-prec(a)} + Fe\text{-prec(a)} \quad (3)$$

$$v\,Ba\text{-prec(a)} + CO_2\ (g) \xrightarrow{air} vBaCO_3 \quad (4)$$

$$(12v)Fe\text{-prec(a)} \xrightarrow{T_1,\ -H_2O\ (g)} (6v)\alpha\text{-}Fe_2O_3 \quad (5)$$

$$(1-v)Ba\text{-prec(a)} + 12(1-v)Fe\text{-prec(a)} \xrightarrow{T_2,\ -H_2O\ (g)} (1-v)BaFe_{12}O_{19} \quad (6)$$

$$vBaCO_3 + v(5z+1)\alpha\text{-}Fe_2O_3 \xrightarrow{T_3,\ -CO_2\ (g)} vzBaFe_{12}O_{19} + v(1-z)BaFe_2O_4 \quad (7)$$

$$5v(1-z)\alpha\text{-}Fe_2O_3 + v(1-z)BaFe_2O_4 \xrightarrow{T_4} v(1-z)BaFe_{12}O_{19} \quad (8)$$

where A stands for a chloride or nitrate group, 'a' denotes the amorphous state, while the other phases are crystalline, and prec denotes a precursor. Note also the variables, $v \leq 1$ and $z \leq 1$, and that $T_1 = 290$ °C, $T_2 = 500$ °C and $T_3 = T_4 = 600$ °C.

The as-coprecipitated precursors were mostly amorphous (Eq. (3)). The Ba-precursor, most probably having the chemical composition of $Ba(OH)_2 \cdot xH_2O$,[8] partially reacted with CO_2 from the air and formed crystalline $BaCO_3$ (Eq. (4)) after the coprecipitation. If $BaCO_3$ was to form quantitatively, the mass loss due to its degradation prior to the formation of BaM would be 3.8%. The mass loss associated with the formation of the BaM is significantly lower (around 1%, see Section 3.2). Therefore, we can conclude that the decomposition of the Ba-precursor and the consequent formation of the $BaCO_3$ were only partial. The Fe precursor partly decomposed into α-Fe_2O_3 (Eq. (5)). During the heating to T_2 (500 °C) BaM crystallizes directly from the amorphous precursors (Eq. (6)). However, the BaM formation is not completed at 500 °C, but it is at 600 °C (Eq. (8)). Obviously, $BaCO_3$ cannot react below T_4 (600 °C). This was confirmed by the TG/MS measurement of the ETcl sample that contained the maximum possible amount of BaM obtainable at 500 °C (calcination 50 h at 500 °C). When this particular sample was heated to 800 °C with a heating rate of 10 K/min, ~1% of the mass loss due to CO_2 evaporation was detected. This is in accordance with the mass loss associated with the DTA peak for the BaM formation (Fig. 2). The degradation of $BaCO_3$ results in the formation of $BaFe_2O_4$ (Eq. (7), Fig. 4) and maybe $BaFe_{12}O_{19}$. At this stage it is not clear if $z > 0$. Finally, at 600 °C $BaFe_2O_4$ reacts with α-Fe_2O_3 (Eq. (8)). This reaction is typical for a pure solid-state synthesis.[9,24] Hence, it is proposed that the formation of BaM using coprecipitation is composed of at least two different mechanisms: (i) the direct formation from amorphous precursors, and (ii) the indirect formation via $BaFe_2O_4$. The dual mechanism for the formation of $BaFe_{12}O_{19}$ results in the formation of particles with a broad size distribution. An example is shown in Fig. 5. Here, well-defined plate-like particles with diameters of more than 100 nm can be observed together with irregularly shaped nm-sized particles.

4.2. The influence of temperature and time on the formation of BaM

Both processing parameters, the solvent and the reagent salts, influenced the kinetics of BaM formation. As described in Section 2, the M/M_{max} values were taken as a quantitative measure

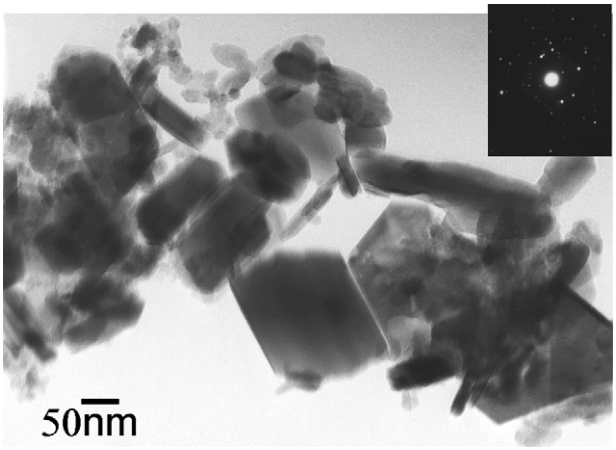

Fig. 5. TEM image of the ETni sample calcined at 600 °C for 10 h with the corresponding electron diffraction pattern.

for the mass fraction (α) of the formed BaM. Therefore, the shape of $\alpha = \alpha(t)$ is the same as that of $M = M(t)$ (Fig. 1). Similar $M = M(t)$ dependences were observed for all three types of samples. A sharp increase in M with no distinct induction period indicates instantaneous nucleation. The temperature strongly influences the BaM formation rate and the overall shape of the $\alpha = \alpha(t)$ curve resembles those typical of diffusion-limited reactions resulting from a deceleratory type of process.[23] Here, the nucleation and the reaction are very rapid at sufficiently high temperatures. The product is formed at the boundary between the reactants and represents a barrier through which the reactants have to diffuse for the continuation of the reaction. From among the most common kinetic models applied to solid-state reactions, the shape of the $\alpha = \alpha(t)$ curves fitted well to the general kinetic equation (Eq. (9)):

$$-\ln(1-\alpha) = (kt)^n \quad (9)$$

The determined kinetic parameters are listed in Table 3. The reaction order (n) varied with the temperature and the type of sample. The n-values were the highest at 500 °C (~1) and decreased with temperature. The reaction-rate constants (k) of all the samples were similar at 500 °C (~10^{-5} s^{-1}) and increased with temperature, exceeding 10^{10} s^{-1} at 800 °C. The temperature's influence on the k-values increased in the same order as the activation energy (E_a): Wcl < ETcl < ETni. The high E_a values indicate that the rate-limiting process is bulk diffusion. There are some differences between the differently determined E_a values: they are lower when determined from the isothermal data (Eqs. (1) + (9)) than when they are determined from the dynamic data (Eq. (2)). And in the latter case, E_a(Wcl) = E_a(ETcl) < E_a(ETni). The difference in the differently determined E_a values can be partly attributed to the errors related to the determination methods and may originate from the experimental error associated with the determination of the k-values (Eq. (1)) or from the assumptions related to the derivation of Eq. (2).[24] However, we believe that the main difference results in the different reactions taking place at different temperatures (Eqs. (6)–(8)), and the following explanation is proposed: The DTA peak corresponding to the formation of BaM (Eq. (2)) does not represent the complete formation of BaM. The formation of BaM starts below the temperature of the corresponding DTA peak at the same time as the decomposition of the precursors (Eq. (6)). Similar findings have been reported previously for the citrate-precursor method.[12,19] The change in enthalpy associated with the decomposition of the precursors must be similar to that associated with the formation of BaM, since no distinct DTA peaks were observed for these processes. The reaction occurs at 500 °C and results in the nearly complete formation of BaM, $\alpha \sim 0.8$. After that the formation of BaM proceeds from the crystalline intermediates (Eqs. (7) and (8)). This corresponds to the high-temperature exothermic DTA peak (Fig. 2) and to the mass loss of ~1%. The E_a for the indirect formation of BaM is higher than the E_a for the direct formation of BaM. Consequently, the indirect formation of BaM takes place at higher temperatures than the direct formation of BaM. All this also explains the discrepancy between the formation temperature of BaM determined from the XRD and from the magnetic measurements, and the formation temperature determined from the DTA (Section 3.2). Hence, it is evident that the formation mechanism of BaM is essentially sensitive to the in situ formation of $BaCO_3$ due to the manipulation of the precursors in air.

Table 3
Kinetic parameters derived from Eqs. (1), (2) and (9)

	Sample		
	Wcl	ETcl	ETni
n (500 °C)	1.3	0.85	0.84
k (500 °C) (s^{-1})	2.3×10^{-5}	1.4×10^{-5}	2.2×10^{-5}
n (600 °C)	0.18	0.54	1.2
k (600 °C) (s^{-1})	6.3×10^{-3}	1.8×10^{-3}	4.9×10^{-4}
n (700 °C)	0.3	0.13	
k (700 °C) (s^{-1})	2.3×10^{-2}	0.25	
k (800 °C)	$>10^{10}$	$>10^{10}$	$>10^{10}$
E_a (Eqs. (1) + (9)) (kJ/mol)	220	299	338
E_a (Eq. (2)) (kJ/mol)	310	310	394

5. Conclusions

The mechanism of $BaFe_{12}O_{19}$ formation via coprecipitation was studied. Samples were prepared by the calcination of precursors coprecipitated from chlorides and nitrates in water or an ethanol solution. The formation of $BaFe_{12}O_{19}$ takes place via two competing processes, regardless of the coprecipitation conditions: directly from amorphous precursors and indirectly via crystalline intermediates. The direct formation of $BaFe_{12}O_{19}$ takes place at lower temperatures due to its lower activation energy than the indirect formation of $BaFe_{12}O_{19}$ with a higher activation energy. It can be concluded that the suppression of the formation of $BaCO_3$ is necessary for the low-temperature formation of the $BaFe_{12}O_{19}$.

Acknowledgement

This work was supported by the Ministry of Higher Education, Science and Technology of Republic of Slovenia and by Iskra Feriti d.o.o.

References

1. Smit, J. and Wijn, H. P. J., *Ferrites, Philips' Technical Library*. Eidenhoven, 1959, pp. 162–211 (Chapters VIII–IX).
2. Went, J. J., Rathenau, G. W., Gorter, E. W. and van Oosterhout, G. W., Ferroxdure a class of new permanent magnet materials. *Philips Technol. Rev.*, 1952, **13**(7), 194–208.
3. Kubo, O., Ido, T. and Yokoyama, H., Properties of Ba ferrite particles for perpendicular magnetic recording media. *IEEE Trans. Magn.*, 1982, **MAG-18**(8), 1122–1124.
4. Rodrigue, G. P., Magnetic materials for millimeter wave applications. *IEEE Trans. Microwave Theory Techn.*, 1963, **MTT-11**, 351–356.
5. Rozman, M. and Drofenik, M., Sintering of nanosized MnZn-ferrite powders. *J. Am. Ceram. Soc.*, 1998, **81**, 1757–1763.
6. Sudakar, C., Subbannna, G. N. and Kutty, T. R. N., Nanoparticles of barium hexaferrite by gel to crystalline conversion and their magnetic properties. *J. Electroceram.*, 2001, **6**(2), 123–134.
7. Haneda, K., Miyakawa, C. and Kojima, H., Preparation of high-coercitivity $BaFe_{12}O_{19}$. *J. Am. Ceram. Soc.*, 1974, **57**(8), 354–357.
8. Roos, W., Formation of chemically coprecipitated barium ferrite. *J. Am. Ceram. Soc.*, 1980, **63**(11/12), 601–603.
9. Carp, O., Barjega, R., Segal, E. and Brezeanu, M., Nonconventional methods for obtaining hexaferrites. II. Barium hexaferrite. *Thermochim. Acta*, 1998, **318**, 57–62.
10. Suerig, C., Hempel, K. A. and Bonnenberg, D., Hexaferrite particles prepared by sol–gel technique. *IEEE Trans. Magn.*, 1994, **30**(6), 4092–4094.
11. Pullar, R. C. and Bhattacharya, A. K., Crystallization of hexagonal M ferrites from a stoichiometric sol–gel precursor, without formation of the α-$BaFe_2O_4$ intermediate phase. *Mater. Lett.*, 2002, **57**, 537–542.
12. Sankaranarayanan, V. K. and Khan, D. C., Mechanism of the formation of nanoscale M-type barium hexaferrite in the citrate precursor method. *J. Magn. Magn. Mater.*, 1996, **153**, 337–346.
13. Ding, J., Maurice, D., Miao, W. F., McCormick, P. G. and Street, R., Hexaferrite magnetic materials prepared by mechanical alloying. *J. Magn. Magn. Mater.*, 1995, **150**, 417–420.
14. Ding, J., Tsuzuki, T. and McCormick, P. G., Ultrafine $BaFe_{12}O_{19}$ powder synthesized by mechanochemical processing. *J. Magn. Magn. Mater.*, 1998, **177–181**, 931–932.
15. Chin, T.-S., Hsu, S. L. and Deng, M. C., Barium ferrite particulates by a salt-melt method. *J. Magn. Magn. Mater.*, 1993, **120**, 64–68.
16. Shirk, B. T. and Buessem, W. R., Magnetic properties of barium ferrite formed by crystallization of a glass. *J. Am. Ceram. Soc.*, 1970, **53**(4), 192–196.
17. Barb, D., Diamandescu, L., Rusi, A., Tarabasanu-Mihaila, D., Morariu, M. and Teodorescu, V., Preparation of barium hexaferrite by a hydrothermal method: structure and magnetic properties. *J. Mater. Sci.*, 1986, **21**, 1118–1122.
18. Padmini, P. and Narayanan Kutty, T. R., Wet chemical syntheses of ultrafine multicomponent ceramic powders through gel to crystalline conversion. *J. Mater. Chem.*, 1994, **4**(12), 1875–1881.
19. Ogasawara, T. and Oliviera, M. A. S., Microstructure and hysteresis curves of the barium hexaferrite from co-precipitation by organic agent. *J. Magn. Magn. Mater.*, 2000, **217**, 147–154.
20. Goto, Y. and Takada, T., Phase diagram of the system BaO–Fe_2O_3. *J. Am. Ceram. Soc.*, 1960, **43**(3), 150–153.
21. Lisjak, D. and Drofenik, M., The low temperature formation of barium hexaferrites. *J. Eur. Ceram. Soc.*, 2006, **26**, 3681–3683.
22. D. Lisjak, M. Drofenik, The influence of the coprecipitation conditions on the low temperature formation of barium hexaferrite. J. Mater. Sci., submitted for publication.
23. Bamford, C. H. and Tipper, C. F. H., *Comprehensive Chemical Kinetics, vol. 22. Reactions in the Solid State*. Elsevier Scientific Publishing Company, Amsterdam, 1980, pp. 41–113 (Chapter 3).
24. Maritta, A. and Buri, A., Kinetics of devitrification and differential thermal analysis. *Thermochim. Acta*, 1978, **25**, 155–160.